Research
Biomedical Engineering—Review

Review of 4Pi Fluorescence Nanoscopy

Xiang Hao [a],[*],[#], Yiming Li [b],[#], Shuang Fu [b], Yanghui Li [c], Yingke Xu [d], Cuifang Kuang [a], Xu Liu [a]

[a] State Key Laboratory of Modern Optical Instrumentation, College of Optical Science and Technology, Zhejiang University, Hangzhou 310027, China
[b] Department of Biomedical Engineering, Southern University of Science and Technology, Shenzhen 518055, China
[c] College of Optical and Electronic Technology, China Jiliang University, Hangzhou 310018, China
[d] Key Laboratory for Biomedical Engineering of Ministry of Education & Zhejiang Provincial Key Laboratory of Cardio-Cerebral Vascular Detection Technology and Medicinal Effectiveness Appraisal, College of Biomedical Engineering and Instrument Science, Zhejiang University, Hangzhou 310027, China

A R T I C L E   I N F O

A B S T R A C T

Since the 1990s, continuous technical and scientific advances have defied the diffraction limit in micro-scopy and enabled three-dimensional (3D) super-resolution imaging. An important milestone in this pur-suit is the coherent utilization of two opposing objectives (4Pi geometry) and its combination with super-resolution microscopy. Herein, we review the recent progress in 4Pi nanoscopy, which provides a 3D, non-invasive, diffraction-unlimited, and isotropic resolution in transparent samples. This review includes both the targeted and stochastic switching modalities of 4Pi nanoscopy. The schematics, principles, appli-cations, and future potential of 4Pi nanoscopy are discussed in detail.

© 2020 THE AUTHORS. Published by Elsevier LTD on behalf of Chinese Academy of Engineering and Higher Education Press Limited Company. This is an open access article under the CC BY-NC-ND license (http://creativecommons.org/licenses/by-nc-nd/4.0/).

1. Introduction

Since the discovery of the diffraction limit by Abbe et al. in 1873 [1], the resolution of far-field optical microscopy has been con-strained by the diffraction of light for over a century. However, the pursuit of higher resolution has been in progress [2], and major breakthroughs have been achieved since the early 1990s [3]. Diffraction limits the resolution of visible light microscopy in resolving objects no closer than 250 nm; however, nanoscopy has overcome this fundamental limit and improved the achievable resolution by up to a factor of ten in the xy-plane and a factor of six along the z-axis. The development of far-field fluorescence nano-scopy has progressed significantly in the past two decades. Nota-bly, fluorescence nanoscopy does not refer to a specific technique. Instead, scientists use this term to describe several dif-ferent modalities as the common underlying basis is the switching effect on fluorescence emission. All fluorescence nanoscopy con-cepts realized hitherto involve the bright ("on") and dark ("off") states of fluorophores to record subdiffraction-limited features sequentially in time [4,5], and the molecular probability of being either in the bright or in dark state depends nonlinearly on the light intensity applied [4]. By either the coordinate-targeted or stochastic temporal switching of fluorophores, these techniques remarkably visualize cellular structures specifically labeled with fluorophores at the subdiffraction-limited scale and thus have enabled the investigation of many fundamental biological phe-nomena with light microscopy for the first time [6].

As most biological structures are arranged three-dimensionally, extending super-resolution imaging to three dimensions is desirable to unambiguously visualize these structures and/or their motions. Hence, several innovative approaches have been developed in this regard. For single-molecule localization microscopy (SMLM) tech-niques, such as photoactivated localization microscopy (PALM) [7], stochastic optical reconstruction microscopy [8], and fluorescence PALM [9], methods for extending imaging from two to three dimen-sions primarily include the simultaneous imaging of two different focal planes [10] or point-spread function (PSF) engineering [11–14]. For coordinate-targeted nanoscopy techniques, such as stimu-lated emission depletion (STED) microscopy [15] and reversible sat-urable optical fluorescence transition (RESOLFT) microscopy [16], the most commonly used strategy is to employ two-phase masks simultaneously to create a three-dimensional (3D) intensity mini-mum in the center of the STED/RESOLFT focus [17,18].

For both techniques, the resolution can be unlimited. However, diffraction is still critical in these "diffraction-unlimited" approaches because their resolution benefits significantly from

* Corresponding author.
  E-mail address: haox@zju.edu.cn (X. Hao).
# These authors contributed equally to this work.

the sharp focusing of light. If light can be focused/collected from only one side of the focal plane, then the diffractive nature of the light stretches the PSF more along the propagation direction of the beam. Consequently, it is more challenging to enhance the resolution in the axial direction when using single-objective microscopes. In practice, the lateral resolution of a nanoscope can be between 20 and 40 nm in the focal plane, whereas the axial resolution is always ~2.5 times greater.

A 3D isotropic resolution is preferred because it offers more natural vision and yields a more precise image-based data analysis. However, as a conventional lens can collect only hemispherical wavefronts, it is extremely difficult to achieve isotropic 3D resolution using a single-objective system without sacrificing the lateral resolution. If an imaging system can collect the other half of the wavefront on the "back side" of the focal plane, producing a (nearly) complete spherical wavefront, then the PSF will be (almost) spherical owing to the restored symmetry. Consequently, isotropic 3D resolution can be achieved. Based on this idea, in the early 1990s, Hell et al. [19,20] introduced a 4Pi microscope equipped with two opposing objectives. One objective can only encompass a maximum semi-aperture angle of approximately 65°, whereas two opposing objectives virtually mimic an aperture with a nearly full solid angle of 4π ($2.5\pi–3\pi$ in practice). In 4Pi microscopy, the counter-propagating wavefronts of the illumination from opposing objectives form interference fringes at the common focal spot (4Pi type A), as shown in Fig. 1. Alternatively, the collected fluorescence may interfere at the detector (4Pi type B). This additional interference around the focal region, which is the essence of scanning 4Pi microscopy, significantly sharpens the PSF along the optical axis. If only excitation (4Pi type A) or emission (4Pi type B) photons are coherent, then this approach can improve the resolution by three to four folds. Sharpening both the excitation and emission PSFs (4Pi type C) further improves the axial resolution up to approximately seven folds [21]. In addition, the 4Pi arrangement can facilitate the doubling of the detected fluorescence, thereby improving the signal-to-noise ratio (SNR) of the image. Similarly, incoherent interference illumination image interference microscopy [22] applies an axial-structured light field to illuminate the sample and coherently collects fluorescence photons through both objectives, thereby attaining a resolution comparable to that of spot-scanning 4Pi microscopy in a wide-field, camera-based imaging architecture.

When combined with fluorescence nanoscopy methods, 4Pi microscopy can acquire images with further improved resolution in three dimensions, particularly in the z-direction. Similar to conventional nanoscopes with one objective, 4Pi nanoscopes can be classified as targeted switching (isoSTED [23]/4Pi-RESOLFT [24]) or stochastic switching (interferometric photoactivated localization microscopy (iPALM) [25]/4Pi-single molecule switching microscopy (SMS) [26]/4Pi-SMLM [27]) modalities, as shown in Fig. 2(a) [23–27]. In the case of the targeted switching modality, the destructive interference of counter-propagated wavefronts allows a much sharper central minimum to be created in the axial direction of the STED/RESOLFT focus (Fig. 2(b) [25–27]); subsequently, the fluorescence emission is confined to the immediate vicinity of the focal spot. The major technical difference that distinguishes 4Pi-RESOLFT from isoSTED is that the former typically uses reversibly switchable fluorescent proteins (RSFPs) to provide mandatory bright and dark states. In the case of the stochastic switching modality, enhanced resolution is realized by converting the phase information hidden in the interference fringes to precise z localization (Fig. 2(b)). Depending on the design of the interference cavity, both three (iPALM [25]) and four (4Pi-SMS [26], 4Pi-SMLM [27]) interference phase images can be recorded simultaneously.

In the following sections, we discuss both the concepts of 4Pi nanoscopy and their applications in detail. By contrast, image-interference and incoherent-illumination-interference structured illumination microscopy (I^5S) [28] is beyond the scope of this review. I^5S expands the application of structured illumination in the lateral direction, compressing the effective PSF both laterally and axially. However, it does not rely on any switching fluorescence effects, either targeted switching or stochastic illumination. This is advantageous because it makes I^5S compatible with almost all types of fluorophores. However, theoretically, I^5S can only double the resolution when using wide-field microscopes as a reference. To further improve the resolution, nonlinear effects such as fluorescence saturation [29–31] are still necessary. However, saturated I^5S (denoted as "I^5SS") is yet to be realized.

2. Targeted switching of 4Pi nanoscopy

STED nanoscopy is based on a scheme developed in 1994 [15] and was first demonstrated in material science in 1999 [32] and subsequently in biology in 2000 [33]; since then, it has
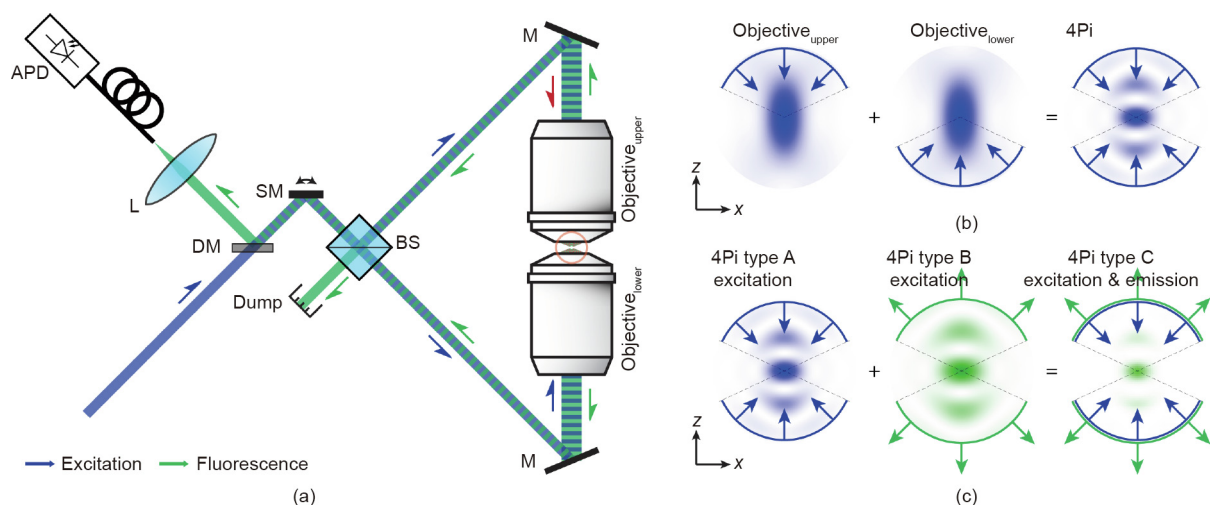

Fig. 1. Simplified schematic and principle of 4Pi microscopy. (a) Simplified schematic of 4Pi microscopy. (b) PSFs in 4Pi nanoscopy in axial (*xz*) plane. Coherent superposition of PSFs from the upper and lower objectives sharpens focal spot size in *z*-axis. (c) Effective PSFs of different 4Pi types. From left to right: 4Pi type A, excitation beams are coherent; 4Pi type B, emission beams (fluorescence) are coherent; 4Pi type C, both are coherent. APD: avalanche photodiode; BS: 50/50 beam splitter; DM: dichroic mirror; L: lens; M: mirror; SM: scanning mirror.

revolutionized fluorescence imaging. It is the first developed nanoscopy technique operating in the targeted switching mode; it restricts fluorescence to a subdiffraction-sized region at known positions by depleting excited fluorophores surrounding it through stimulated emissions. A peak-centered excitation focal spot, nested by a ring-shaped depletion focus, is scanned across the sample, and the image is generated by reading out signals from a point detector conjugated to the focus. To improve the resolution of the STED method, fluorescence emission must be inhibited everywhere except at the center of the depletion focus; therefore, a high quality "zero"-intensity point in the center of the ring-shaped depletion pattern is mandatory [34].

Technical advances in the past 15 years have enabled a new era of 3D imaging in STED nanoscopy. In particular, using two opposing objectives in a 4Pi geometry allows a sharp central minimum to be created in the axial direction of the depletion focus. It has enabled a 33 nm z-resolution [35] despite the insufficient resolution improvement in "STED-4Pi microscopy" [35,36] in the focal plane. An improved version of this method, isoSTED nanoscopy [23], has demonstrated 3D isotropic resolution (Fig. 2(a)). To isotropically compress fluorescence, isoSTED nanoscopy utilizes two depletion patterns featuring a common focal zero: one for lateral (STED$_{xy}$) and another for axial depletion (STED$_z$), as shown in Fig. 2(b). Adjusting the power allocation between these two patterns enables a precise control of the PSF size and hence the resolution. Specifically, the formation of the STED$_z$ depletion profile relies on the superposition of the waves emerging from the two objectives propagating in opposite directions. Owing to the highly symmetric intensity and phase distribution of the single-objective PSF with respect to the focal plane, in addition to the central "zero"-intensity point, the destructive interference of the waves yields axially repetitive minima above and below the focal plane
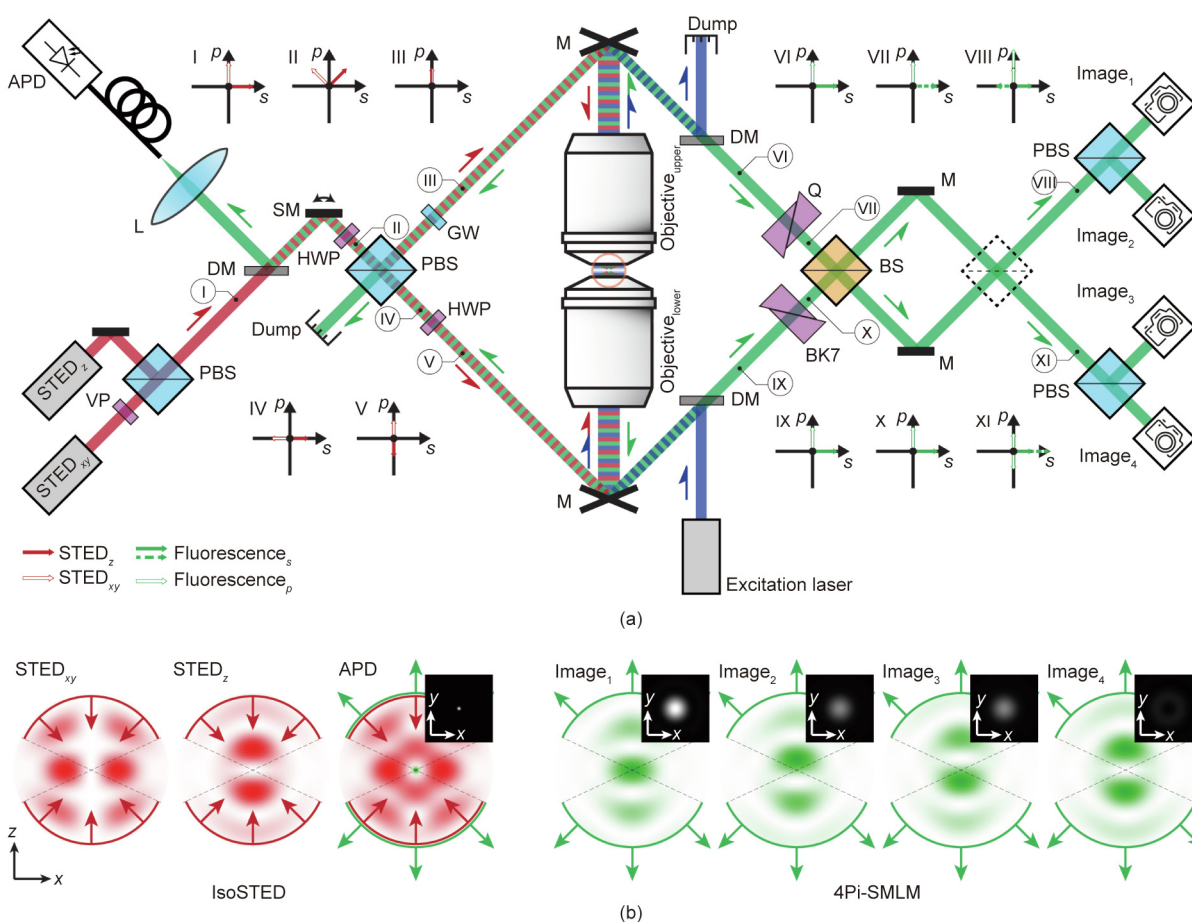

Fig. 2. Simplified schematic and principle of 4Pi nanoscopy. (a) Simplified schematic of isoSTED/4Pi-RESOLFT (left) and 4Pi-SMLM nanoscopes (right). For both modalities, the sample is mounted between two opposing objectives. The polarization states at indicated points (I–XI in circles) are displayed around the beam path. Specifically, in VII, VIII, and XI, dashed arrows represent an additional $\pi/2$ phase (introduced by quartz wedges) delay with respect to the solid arrows along the same direction. Left: In an isoSTED/4Pi-RESOLFT nanoscope, the beams for STED$_{xy}$ (lateral) and STED$_z$ (axial) are combined by a polarizing beam splitter (PBS) and then fed through a scanning mirror unit into a 4Pi cavity. STED$_{xy}$ and STED$_z$ beams are incoherent and orthogonal in the polarization direction. Incoming beams are further split by the second PBS and generate STED$_{xy}$ and STED$_z$ depletion patterns (the first and the second panels from left in (b), respectively) at the common focus of the opposing objectives. These two patterns feature the same focal zero in terms of intensity. Their superimposition enables isotropic fluorescence compression by stimulated emission (the third panel from left in (b)), for which the fluorophores underneath the STED patterns are forced to reside in the dark ("off") state. The fluorescence from the immediate vicinity of the focus is inversely collected by the same objectives, reflected by a dichroic mirror, and finally collected by the detector(s). Right: In a 4Pi-SMLM nanoscope, the fluorescence is split and recombined by a set of beam splitters to create partial wavefronts with different interference phases. The interference wavefronts are then simultaneously detected by the cameras after the interference cavity. Whereas the exact beam path and number of detectors may vary in different designs [25–27], the principle for molecule localization is identical: As the fringe-like interference 4Pi-PSF contains more high-frequency information, the resulting localization precision of 4Pi-PSF is higher than that of single-objective PSF. (b) PSFs in 4Pi nanoscopy in axial (xz) plane. From left to right: STED$_{xy}$, STED$_z$, combined STED (red) and effective (green) PSFs in isoSTED/4Pi-RESOLFT nanoscopy; fluorescence PSFs with $\varphi = 0$, 90°, 270°, and 180° in 4Pi-SMLM nanoscopy. For a clear depiction of the effective PSF in isoSTED/4Pi-RESOLFT nanoscopy and fluorescence PSFs in 4Pi-SMS nanoscopy, the detected images on the detectors (APD or cameras) in the focal (xy) plane are presented on the top-right corners of the corresponding PSFs. GW: glass window; HWP: half wave plate; Q: quartz wedge; VP: 0–2π vortex phase plate; s/p: s-/p-polarization.

in the STED$_z$ profile, overlapping with the excitation and detection PSFs. These minima, which theoretically correspond to zero intensity, prevent fluorescence depletion at their locations, resulting in side-lobes in the effective PSF. These side-lobes create artifacts, that is, "ghost images," which deteriorate the image quality significantly. Furthermore, when the sample is scanned in the axial direction, the positions of the maxima shift under the PSF envelope; thus, any deconvolution procedure based on a spatially invariant PSF is rendered futile. In principle, deconvolution with a variable PSF [37] can mitigate this phenomenon; however, the method relies on accurate knowledge regarding the PSF and is only applicable to images with good SNRs. To eliminate axial side-lobes in an effective PSF, an effective strategy is to apply defocusing to shift the foci of both objectives and create an axial misalignment between the two opposing STED$_z$ focal spots [38]. By performing the proposed phase manipulation using a phase mask, the disadvantages of an alternative method involving misaligning the two opposing objectives can be avoided, namely, reduced fluorescence signal and poor lateral resolution [38]. Similar to the STED$_z$ pattern, the STED$_{xy}$ pattern is generated by the opposing propagating beams in a constructive interference manner. Remarkably, although the intensity profile and total STED power are generally unchanged with respect to the single-objective modality, the additional interference can double the peak intensity, equivalent to a resolution enhancement of $\sqrt{2}$ times based on the modified Abbe's equation [39].

The ability of isoSTED nanoscopy in confining the fluorescence to the immediate vicinity of the focus creates an effective PSF that is 1500 times smaller than that of the confocal one, implying a resolution of 20–50 nm in three dimensions [23]. The significant gain over the confocal PSF renders isoSTED nanoscopy a powerful noninvasive methodology for the 3D imaging of transparent samples at the nanoscale. The applications of isoSTED nanoscopy have been demonstrated in multiple disciplines. Immediately after invention, an isoSTED nanoscope was applied in material science to image self-assembled nanostructures [40]. These structures are formed by a block copolymer system (styrene-*block*-2-vinylpyridine, Fig. 3(a) [40]), in which the vinylpyridine phase is specifically labeled with Atto 647N to provide fluorescence contrast. The resultant image of the confocal microscope (Fig. 3(b) [40]) does not show any features of the swelling-induced morphology, whereas, the isoSTED nanoscope provides more underlying information (Fig. 3(c) [40]). In particular, the unique strength of the isoSTED nanoscope enables a noninvasive visualization of the complete 3D structure within the sample bulk, which was previously inaccessible via electron microscopes.

In addition to material science, the emerging importance of isoSTED nanoscopy is exemplified in cell biology. Mitochondrion, an organelle with a fundamental role in energy production, is the first imaging target of the isoSTED nanoscope. Mitochondria are bounded by two different membranes and have a typical diameter of 200–400 nm, as first revealed by electron microscopy (EM) in

the 1950s [41] (Fig. 4(a) [42]). The development of isoSTED nanoscopy has enabled scientists to analyze nanoscale biological structures. By scanning a ~35 nm-diameter PSF throughout the mitochondria, isoSTED nanoscopy has successfully mapped the distribution of both F$_1$F$_0$-adenosine triphosphate synthase (ATPase) (Fig. 4(b) [42,43]) and translocase of the outer mitochondrial membrane member 20 (TOMM20) (Fig. 4(c) [23,42,43]). In another demonstration, scientists focused on synaptic vesicles [42], that is, small, electron-lucent vesicles with an average diameter of 39.5 nm [44]. These synaptic vesicles, which reside in presynaptic terminals, store neurotransmitters and are essential for propagating nerve impulses between neurons. Benefitting from the ability of isoSTED nanoscopy, the spatial distribution of the surface pool in the periactive zone of the hippocampal boutons was successfully resolved.

Despite the stronger sectioning capability of isoSTED nanoscopy over ordinary STED nanoscopy, the power level of the depletion laser required by isoSTED nanoscopy is extremely high for most living specimens. To enable live-cell imaging using 4Pi nanoscopy, 4Pi-RESOLFT was developed [24]. As an isoSTED-derivative, 4Pi-RESOLFT typically replaces fluorescent dyes with RSFPs to provide "on" and "off" states. RSFP-based RESOLFT is particularly attractive because it operates at a low laser power (approximately two orders of magnitude lower than that required for isoSTED nanoscopy [24]), rendering it more compatible for living cells.

3. Stochastic switching of 4Pi nanoscopy

The optical resolution of SMLM has reached a few nanometers, thus enabling the optical analysis of nanobiostructures [45]. It utilizes wide-field excitation and detection to stochastically excite and precisely localize single molecules, achieving superresolution capability. This approach is currently widely used as it is easy to implement in conventional wide-field setups [46]. The 3D-SMLM is typically implemented by evaluating the PSF with
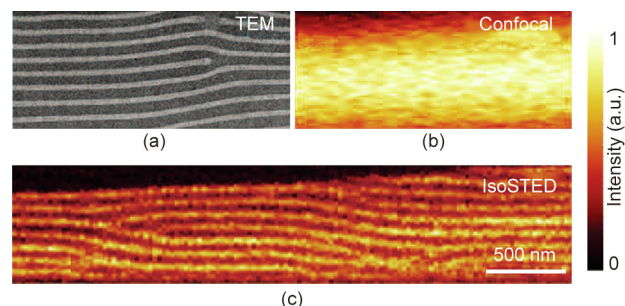

Fig. 3. Application of isoSTED nanoscopy in material science. (a) Transmission electron micrograph (TEM) of solvent-annealed thin film showing lamellar structure. (b) Confocal image of block copolymer is featureless, whereas (c) isoSTED image clearly reveals the underlying morphology. a.u.: arbitrary unite. Reproduced form Ref. [40] with permission of American Chemical Society, © 2009.
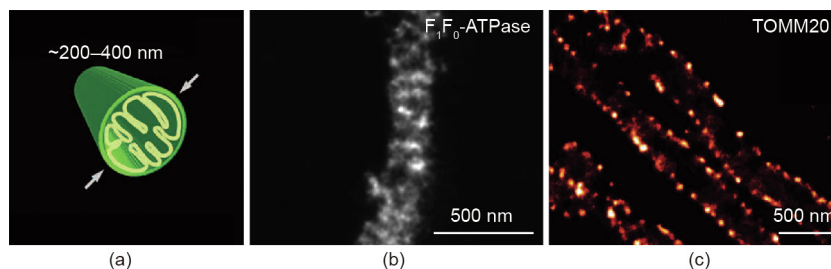

Fig. 4. Application of isoSTED nanoscopy in cell biology. (a) Dimensions of mitochondrial tubule. IsoSTED image of (b) F$_1$F$_0$-ATPase and (c) TOMM20 in wild-type PtK2 cells. Reproduced form Ref. [43] with permission of ACS, © 2009.

lateral information as well as with the PSF shape [11–14]. Alternatively, the axial position of individual molecules can be retrieved by simultaneously imaging multiple focal planes [10]. Depending on the detected photons, this technique can achieve a lateral resolution of 20–30 nm, whereas the axial resolution is typically several-fold worse.

Compared with the conventional single-objective 3D-SMLM system, 4Pi-SMLM uses the interference of fluorescence signals detected by two opposing objectives to increase the z-resolution significantly. The two opposing objectives collect the (almost) complete spherical wavefront, thereby doubling the number of detected photons and increasing the aperture angle. Furthermore, overlaying both detection paths can result in the self-interference of individual photons when the optical path length of the two axial imaging paths is within the coherent length. Single molecules with three [25] or four [26,27] interference phases are then simultaneously recorded. As the interference phase is highly sensitive to the fluorophore's axial position, the resulting axial resolution is approximately six to ten times higher than the axial resolution achievable using the single-objective system, surpassing the lateral resolution in some cases.

The axial resolution for single-objective nanoscopy can reach ~60 nm [11], but bright synthetic fluorophores are required. The performance obtained using dimmer fluorescent proteins (FPs) is typically poorer [47]. By contrast, 3D sub-10 nm resolution is theoretically achievable in 4Pi-SMLM with only 250 photons collected in each objective for an individual fluorophore [48]. Therefore, 4Pi-SMLM is suitable for imaging biological samples labeled with dimmer photoactivatable fluorescent proteins (PA-FPs). Endogenously expressed PA-FPs offer several key advantages over synthetic fluorophores [49], particularly in live-cell imaging. They can be fixed more gently as only mild fixation is required, and the cells are returned to the physiological media. In contrast to synthetic fluorophores, oxygen scavenging imaging buffers, potentially perturbative detergents, or treatments are not required to control the photophysics of single molecules.

With an overall resolution of < 20 nm in three dimensions for dimmer PA-FPs, 4Pi-SMLM enables biologists to observe more detailed biological samples in three dimensions. Cell focal adhesions (FAs) that link the extracellular matrix to the actin cytoskeleton are crucial in morphogenesis, immunity, and wound healing [50]. FAs form small (< 250 nm) clustered integrins, focal adhesion kinase, and paxillin during cell edge protrusion. The multilaminar protein architecture of FAs is critical for understanding their functions. Combining 4Pi-SMLM with PA-FP-labeled FAs is an ideal approach for imaging the 3D architecture of different protein composites in FAs. Utilizing the 3D isotropic nanometer resolution capability of 4Pi-SMLM, Kanchanawong et al. [50] discovered that the vertical distributions of each FA component are highly consistent across FAs of different sizes and shapes, suggesting that the position of proteins within FAs regulates their activity and function. Using a similar strategy, Case et al. [51] regulated vinculin activation and function.

Furthermore, 4Pi-SMLM offers quantitative biological insights into many different biological systems, particularly those requiring ultrahigh resolutions [52–56]. The nanoscale organization of endosomal sorting complexes required for transport (ESCRT) machinery, which is hijacked by the human immunodeficiency virus (HIV), was resolved at the virus budding site. The spatial architecture of the ESCRT subunits suggests that the driving force for HIV release may be derived from the initial scaffolding of ESCRT subunits within the viral bud interior [54]. Two discrete barrel structures, each composed of dozens of individual Nup188 clusters, were resolved at the cilium base. The structural details support the concept that Nup199 encapsulates the centrioles within a barrel-like structure [56]. Furthermore, the 3D 4Pi-SMLM image

was applied to quantify the number of proteins in the secretion machinery [52]. Zhang et al. [52] demonstrated 3D molecular clusters of various sizes formed by a secretion system protein, PrgH, near the cell membrane of a bacterium (Fig. 5 [52]). Recently, 4Pi-SMLM has been successfully used to resolve the 3D organization of heterogeneous nanoscale crosslinks, providing insights into the kinetics of microgel formation [57].

In addition to the application in biology and material science, 4Pi-SMLM has evolved progressively and currently offers more imaging capabilities. When the 4Pi-SMLM concept was initially realized, the imaging depth was limited to the z range of one interference period (half of the emission wavelength, ~250 nm). This is because the intensity of the interference is periodic, and intensity peaks belonging to the adjacent interferometric fringes cannot be distinguished. Two methods have been applied to solve this problem. The first method addresses this by introducing astigmatism to the 4Pi-PSF [58]. Therefore, the overall shape of the PSF can be used to unwrap the interference phases in different periods, extending the imaging z depth to the extent afforded by the astigmatic-based 3D-SMLM method (~1 µm). The second method utilizes the concept wherein the emitted wavefronts are spherical rather than planar, and different oscillations of the zeroth and third central moments are investigated to precisely determine the z-position in different periods [26]. Recently, adaptive optics have been introduced to 4Pi-SMLM, enabling whole-cell imaging (Fig. 6 [27]). Additionally, multicolor imaging has been introduced in 4Pi-SMLM; two-color 4Pi-SMLM imaging was first realized by attributing fluorophore color identity with the ratio of s-polarized versus p-polarized emission components [27]. Recently, three-color 4Pi-SMLM was realized using salvaged fluorescence reflected by an excitation dichroic mirror [59]. Another exciting development is correlative 4Pi-SMLM-EM imaging. The high resolution and high molecular specificity of 4Pi-SMLM combined with EM substantially reduced the resolution gap between fluorescence microscopy and EM, providing a much better overlaying of fluorescence signals with EM images [60,61].

In contrast to single-objective 3D-SMLM, in which the theoretical limited resolution is achieved by maximum likelihood estimation using a bead-calibrated experimental PSF model [62], the conventional photometry-based 4Pi-SMLM data analysis workflow fails to reach the theoretical resolution limit [25–27]. This is because the photometry-based method does not exploit the resolution gain from high-frequency information in the fringe-like interference 4Pi-PSF. The development of the cubic-spline-interpolated phase-retrieved 4Pi-PSF model can potentially reach the theoretical resolution limit presented in Ref. [63]. However, 4Pi-PSF is intrinsically four dimensional (x, y, z, and phase). A simple multichannel 3D-PSF model is not well suited for describing the 4Pi-PSF. A recent
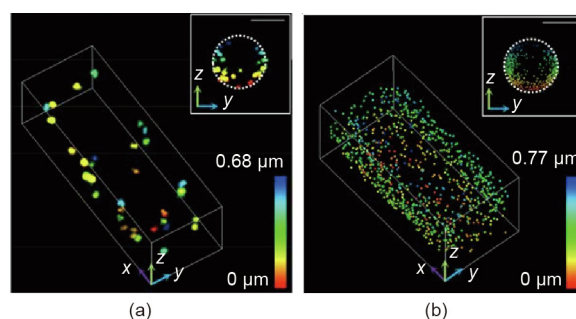

Fig. 5. Ultrahigh resolution 3D imaging of different biological samples using 4Pi-SMLM. (a) 3D imaging of molecular clusters formed by secretion system protein PrgH near bacterial cell membrane. (b) Accumulated 4Pi-SMLM images of PrgH clusters from 58 bacterial cells. Reproduced form Ref. [52] with permission of National Academy of Science, © 2017.
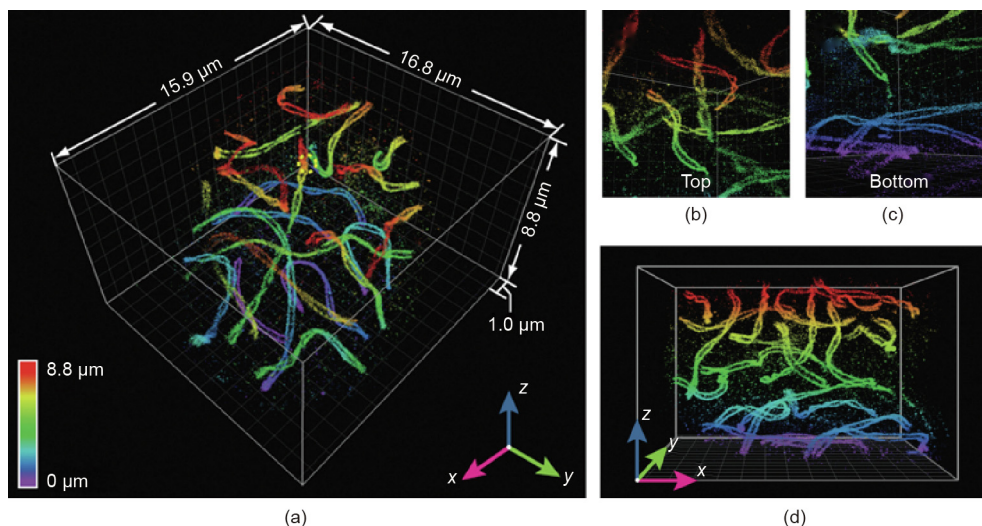
Fig. 6. 4Pi-SMLM imaging of synaptonemal complexes in whole-mouse spermatocyte. (a) Overview images of whole cell reconstructed from 21 optical sections. 4Pi-SMLM images of (b) top and (c) bottom locations inside the spermatocyte. (d) x–z view of (a). Reproduced form Ref. [27] with permission of Elsevier, © 2016.

4Pi-PSF model proposed by Li et al. [64] decoupled the phase term from the 3D position of the 4Pi-PSF. Instead of using a four-dimensional 4Pi-PSF, three 3D-matrices in combination with a simple phase term were used to fully describe the four-dimensional 4Pi-PSF, rendering the calibration of an experimental 4Pi-PSF much easier in practice. Therefore, it can potentially reach the full potential of 4Pi-SMLM.

4. Discussion and outlook

Optical nanoscopy has proven to be an effective technique for investigating the molecular details of subcellular structures via specifically targeted fluorescent labels [45]. It has evolved continually to provide multicolor, 3D, and live-cell imaging with nanometer-scale resolution. In particular, the highlights of all milestones in 4Pi microscopy and nanoscopy are shown in Fig. 7. Most conventional optical nanoscopes offer a resolution in the range of 50–100 nm; however, a further resolution improvement by a factor of ten would enable the 3D imaging of the molecular basis of macromolecular assemblies. This would enable biologists to directly visualize the structure and composition of molecular machinery of cells *in situ*; for example, 3D observations of DNA conformation at such resolutions would be critical for understanding chromosomal DNA packaging and gene regulation [65]. This can be realized by a two-order increase in the number of photons

from single fluorescent emitters in stochastic switching nanoscopy or two orders of increase in depletion laser intensity in targeted switching nanoscopy. However, such a large increase in photons/intensity is typically unfavorable for practical biological experiments. By contrast, dual-objective 4Pi microscopy can substantially augment the 3D resolution of almost all single-objective far-field optical nanoscopy techniques by a three- to ten-fold improved z-resolution. It may be feasible to improve the resolution by an order of magnitude without additional requirements to satisfy the stringent properties of fluorescent labels or harsh imaging conditions.

In addition to 4Pi nanoscopy, other schemes can be used to improve the axial resolution to the sub-50 nm level. For example, point accumulation may be employed for imaging nanoscale topography (PAINT) [66] or its extension, DNA-PAINT [67,68], which replaces the stochastic photoactivation of a permanently bound fluorophore with the stochastic binding of a fluorescent ligand during sample preparation. Another approach that improves the final resolution via sample preparation is expansion microscopy (ExM) [69,70]. By physically enlarging an organism using an expandable polymer network, ExM allows investigators to identify small structures within specimens. In terms of instrumentation, minimal photon fluxes (MINFLUX) is the cutting-edge method for precisely localizing fluorophore molecules [71,72]. In contrast to the classic SMLM that establishes molecule
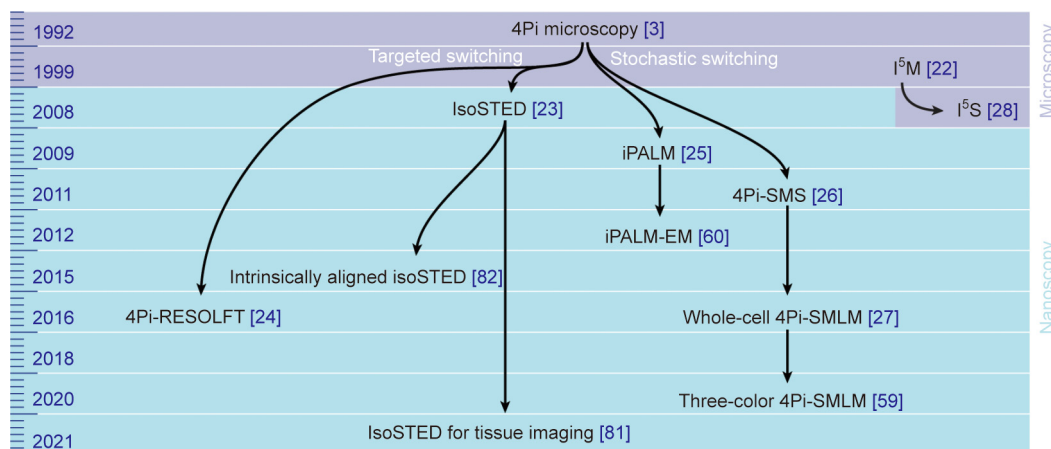

Fig. 7. Instrumental milestones in 4Pi microscopy and 4Pi nanoscopy.

locations by obtaining the centroid or maximum of sparse diffraction-limited emission spots, MINFLUX probes each location with an excitation minimum. Alternatively, the recent development of artificial intelligence offers another route for transforming diffraction-limited input images into super-resolved ones [73] or to significantly reduce the illumination light doses for super-resolution live-cell imaging [74].

To date, the effects of these newly emerging techniques are primarily verified on single-objective arrangements via both microscopy and nanoscopy [71,75–79]. Notably, a fundamental barrier that rejects their integration into setups with two opposing objectives does not exist. One may expect them to provide benefits (higher 3D resolution, better SNR, etc.) similar to those of isoSTED or 4Pi-SMLM by using the 4Pi architecture. However, the major challenge is the increased system complexity: The 4Pi architecture requires a meticulous alignment with a large number of parameters in parallel, in addition to the additional system optimization required specifically for these new concepts. This issue severely compromises the system performance if it is not addressed appropriately. In fact, most 4Pi microscopes/nanoscopes are accessible only in advanced laboratories. A blue print of the 4Pi microscopes, together with open-source software and more operation protocols [80], will enable non-experts to use 4Pi nanoscopy to achieve a substantial resolution enhancement. Scientists endeavoring to simplify the setup of 4Pi nanoscopes have achieved remarkable progress. For example, in the initial setup design of the isoSTED nanoscope, two independent STED beams were implemented to generate $STED_{xy}$ and $STED_z$ profiles. Apparently, an isoSTED setup with one STED beam can potentially reduce the complexity and improve the mechanical robustness. Hence, two ideas were proposed: One is to introduce a double-pass spatial light modulator configuration to encode separate phase profiles for each polarization component [81], and another option is to insert a segmented and chromatic wave plate [82]. Both designs have been realized and proven to facilitate routine isoSTED imaging effectively.

Regarding the high symmetry of the 4Pi interference cavity, a more "aggressive" idea is to completely remove the opposing objectives and use a flat mirror to replace the slide behind the sample in mirror-enhanced super-resolution microscopy (MEANS) [83]. Therefore, the incident and reflected light can mimic the opposing propagating beams in 4Pi nanoscopes, creating local interference on the mirror surface and confine the PSF in the axial direction. Initially, MEANS improved the z-resolution only in a two-dimensional (2D)-STED nanoscope. However, its importance is highlighted by its potential in benefitting both targeted and switching nanoscopies [84]. It provides a general strategy to improve the axial resolution of a single-objective nanoscope, providing access to 4Pi nanoscopy to more laboratories in a virtual manner.

As different 4Pi super-resolution instruments have been well established, the next research focus will be on their applications to address scientific questions. The coherent use of two opposing objectives is the most effective approach if the sample is transparent and accessible from both sides. To maintain a stable interference pattern within the entire imaging process, 4Pi nanoscopy responds sensitively to aberrations induced by refractive index inhomogeneities within the sample. Although 4Pi nanoscopy is scarcely reported for cell imaging, its applications to thick samples, for example, tissues, are almost unexplored. To fully understand aberrations effects, a mathematical model that can describe aberrations in the 4Pi system with two noncontiguous circular pupils [85] is required. Hence, adaptive optics [86] should be introduced to compensate for sample-induced aberrations. This concept has inspired several researchers to conduct pioneering studies to demonstrate 4Pi imaging in whole cells [27] and tissue slices [81]. Although the applications of 4Pi imaging for thick specimens have begun, the full realization of their potential is yet to be realized. The extension of 4Pi imaging to living specimens will be critical to this process.

Acknowledgments

Compliance with ethics guidelines

Xiang Hao, Yiming Li, Shuang Fu, Yanghui Li, Yingke Xu, Cuifang Kuang, and Xu Liu declare that they have no conflict of interest or financial conflicts to disclose.

References

[1] Abbe E. Beiträge zur Theorie des Mikroskops und der mikroskopischen Wahrnehmung. Archiv für Mikroskopische Anatomie 1873;9(1):413–8. German.
[2] Hao X, Kuang C, Gu Z, Wang Y, Li S, Ku Y, et al. From microscopy to nanoscopy via visible light. Light Sci Appl 2013;2(10):e108.
[3] Hell S, Stelzer EHK. Properties of a 4Pi confocal fluorescence microscope. J Opt Soc Am A 1992;9(12):2159–66.
[4] Hell SW. Far-field optical nanoscopy. Science 2007;316(5828):1153–8.
[5] Xu Y, Melia TJ, Toomre DK. Using light to see and control membrane traffic. Curr Opin Chem Biol 2011;15(6):822–30.
[6] Sahl SJ, Hell SW, Jakobs S. Fluorescence nanoscopy in cell biology. Nat Rev Mol Cell Biol 2017;18(11):685–701.
[7] Betzig E, Patterson GH, Sougrat R, Lindwasser OW, Olenych S, Bonifacino JS, et al. Imaging intracellular fluorescent proteins at nanometer resolution. Science 2006;313(5793):1642–5.
[8] Rust MJ, Bates M, Zhuang X. Sub-diffraction-limit imaging by stochastic optical reconstruction microscopy (STORM). Nat Methods 2006;3(10):793–6.
[9] Hess ST, Girirajan TPK, Mason MD. Ultra-high resolution imaging by fluorescence photoactivation localization microscopy. Biophys J 2006;91(11):4258–72.
[10] Juette MF, Gould TJ, Lessard MD, Mlodzianoski MJ, Nagpure BS, Bennett BT, et al. Three-dimensional sub-100 nm resolution fluorescence microscopy of thick samples. Nat Methods 2008;5(6):527–9.
[11] Huang B, Wang W, Bates M, Zhuang X. Three-dimensional super-resolution imaging by stochastic optical reconstruction microscopy. Science 2008;319(5864):810–3.
[12] Pavani SRP, Thompson MA, Biteen JS, Lord SJ, Liu N, Twieg RJ, et al. Three-dimensional, single-molecule fluorescence imaging beyond the diffraction limit by using a double-helix point spread function. Proc Natl Acad Sci USA 2009;106(9):2995–9.
[13] Shechtman Y, Sahl SJ, Backer AS, Moerner WE. Optimal point spread function design for 3D imaging. Phys Rev Lett 2014;113(13):133092.
[14] Baddeley D, Cannell MB, Soeller C. Three-dimensional sub-100 nm super-resolution imaging of biological samples using a phase ramp in the objective pupil. Nano Res 2011;4(6):589–98.
[15] Hell SW, Wichmann J. Breaking the diffraction resolution limit by stimulated emission: stimulated-emission-depletion fluorescence microscopy. Opt Lett 1994;19(11):780–2.
[16] Hofmann M, Eggeling C, Jakobs S, Hell SW. Breaking the diffraction barrier in fluorescence microscopy at low light intensities by using reversibly photoswitchable proteins. Proc Natl Acad Sci USA 2005;102(49):17565–9.
[17] Harke B, Ullal CK, Keller J, Hell SW. Three-dimensional nanoscopy of colloidal crystals. Nano Lett 2008;8(5):1309–13.
[18] Wildanger D, Medda R, Kastrup L, Hell SW. A compact STED microscope providing 3D nanoscale resolution. J Microsc 2009;236(1):35–43.
[19] Hell SW, Stelzer EHK. Properties of a 4Pi confocal fluorescence microscope. J Opt Soc Am A 1992;9(12):2159–66.
[20] Hell SW, inventor; Hell SW, assignee. Doppelkonfokales Rastermikroskop. German patent DE4040441A. 1992 Jul 2.
[21] Bewersdorf J, Schmidt R, Hell SW. Comparison of I5M and 4Pi-microscopy. J Microsc 2006;222(Pt 2):105–17.
[22] Gustafsson MG, Agard DA, Sedat JW. I5M: 3D widefield light microscopy with better than 100 nm axial resolution. J Microsc 1999;195(Pt 1):10–6.
[23] Schmidt R, Wurm CA, Jakobs S, Engelhardt J, Egner A, Hell SW. Spherical nanosized focal spot unravels the interior of cells. Nat Methods 2008;5(6):539–44.

[24] Böhm U, Hell SW, Schmidt R. 4Pi-RESOLFT nanoscopy. Nat Commun 2016;7(1):10504.

[25] Shtengel G, Galbraith JA, Galbraith CG, Lippincott-Schwartz J, Gillette JM, Manley S, et al. Interferometric fluorescent super-resolution microscopy resolves 3D cellular ultrastructure. Proc Natl Acad Sci USA 2009;106(9):3125–30.

[26] Aquino D, Schönle A, Geisler C, Middendorff CV, Wurm CA, Okamura Y, et al. Two-color nanoscopy of three-dimensional volumes by 4Pi detection of stochastically switched fluorophores. Nat Methods 2011;8(4):353–9.

[27] Huang F, Sirinakis G, Allgeyer ES, Schroeder LK, Duim WC, Kromann EB, et al. Ultra-high resolution 3D imaging of whole cells. Cell 2016;166(4):1028–40.

[28] Shao L, Isaac B, Uzawa S, Agard DA, Sedat JW, Gustafsson MG. I⁵S: wide-field light microscopy with 100-nm-scale resolution in three dimensions. Biophys J 2008;94(12):4971–83.

[29] Visscher K, Brakenhoff GJ, Visser TD. Fluorescence saturation in confocal microscopy. J Microsc 1994;175(2):162–5.

[30] Yamanaka M, Saito K, Smith NI, Kawata S, Nagai T, Fujita K. Saturated excitation of fluorescent proteins for subdiffraction-limited imaging of living cells in three dimensions. Interface Focus 2013;3(5):20130007.

[31] Gustafsson MGL. Nonlinear structured-illumination microscopy: wide-field fluorescence imaging with theoretically unlimited resolution. Proc Natl Acad Sci USA 2005;102(37):13081–6.

[32] Klar TA, Hell SW. Subdiffraction resolution in far-field fluorescence microscopy. Opt Lett 1999;24(14):954–6.

[33] Klar TA, Jakobs S, Dyba M, Egner A, Hell SW. Fluorescence microscopy with diffraction resolution barrier broken by stimulated emission. Proc Natl Acad Sci USA 2000;97(15):8206–10.

[34] Hao X, Kuang C, Wang T, Liu X. Effects of polarization on the de-excitation dark focal spot in STED microscopy. J Opt 2010;12(11):115707.

[35] Dyba M, Hell SW. Focal spots of size λ/23 open up far-field fluorescence microscopy at 33 nm axial resolution. Phys Rev Lett 2002;88(16):163901.

[36] Dyba M, Jakobs S, Hell SW. Immunofluorescence stimulated emission depletion microscopy. Nat Biotechnol 2003;21(11):1303–4.

[37] Baddeley D, Carl C, Cremer C. 4Pi microscopy deconvolution with a variable point-spread function. Appl Opt 2006;45(27):7056–64.

[38] Hao X, Allgeyer ES, Booth MJ, Bewersdorf J. Point-spread function optimization in isoSTED nanoscopy. Opt Lett 2015;40(15):3627–30.

[39] Harke B, Keller J, Ullal CK, Westphal V, Schönle A, Hell SW. Resolution scaling in STED microscopy. Opt Express 2008;16(6):4154–62.

[40] Ullal CK, Schmidt R, Hell SW, Egner A. Block copolymer nanostructures mapped by far-field optics. Nano Lett 2009;9(6):2497–500.

[41] Ernster L, Schatz G. Mitochondria: a historical review. J Cell Biol 1981;91(3):227s–55s.

[42] Hua Y, Sinha R, Thiel CS, Schmidt R, Hüve J, Martens H, et al. A readily retrievable pool of synaptic vesicles. Nat Neurosci 2011;14(7):833–9.

[43] Schmidt R, Wurm CA, Punge A, Egner A, Jakobs S, Hell SW. Mitochondrial cristae revealed with focused light. Nano Lett 2009;9(6):2508–10.

[44] Qu L, Akbergenova Y, Hu Y, Schikorski T. Synapse-to-synapse variation in mean synaptic vesicle size and its relationship with synaptic morphology and function. J Comp Neurol 2009;514(4):343–52.

[45] Sigal YM, Zhou R, Zhuang X. Visualizing and discovering cellular structures with super-resolution microscopy. Science 2018;361(6405):880–7.

[46] Schermelleh L, Ferrand A, Huser T, Eggeling C, Sauer M, Biehlmaier O, et al. Super-resolution microscopy demystified. Nat Cell Biol 2019;21(1):72–84.

[47] Shtengel G, Wang Y, Zhang Z, Goh WI, Hess HF, Kanchanawong P. Imaging cellular ultrastructure by PALM, iPALM, and correlative iPALM-EM. Methods Cell Biol 2014;123:273–94.

[48] Von Middendorff C, Egner A, Geisler C, Hell SW, Schönle A. Isotropic 3D Nanoscopy based on single emitter switching. Opt Express 2008;16(25):20774–88.

[49] Shroff H, Galbraith CG, Galbraith JA, White H, Gillette J, Olenych S, et al. Dual-color superresolution imaging of genetically expressed probes within individual adhesion complexes. Proc Natl Acad Sci USA 2007;104(51):20308–13.

[50] Kanchanawong P, Shtengel G, Pasapera AM, Ramko EB, Davidson MW, Hess HF, et al. Nanoscale architecture of integrin-based cell adhesions. Nature 2010;468(7323):580–4.

[51] Case LB, Baird MA, Shtengel G, Campbell SL, Hess HF, Davidson MW, et al. Molecular mechanism of vinculin activation and nanoscale spatial organization in focal adhesions. Nat Cell Biol 2015;17(7):880–92.

[52] Zhang Y, Lara-Tejero M, Bewersdorf J, Galán JE. Visualization and characterization of individual type III protein secretion machines in live bacteria. Proc Natl Acad Sci USA 2017;114(23):6098–103.

[53] Sochacki KA, Larson BT, Sengupta DC, Daniels MP, Shtengel G, Hess HF, et al. Imaging the post-fusion release and capture of a vesicle membrane protein. Nat Commun 2012;3(1):1154.

[54] Van Engelenburg SB, Shtengel G, Sengupta P, Waki K, Jarnik M, Ablan SD, et al. Distribution of ESCRT machinery at HIV assembly sites reveals virus scaffolding of ESCRT subunits. Science 2014;343(6171):653–6.

[55] Buss J, Coltharp C, Shtengel G, Yang X, Hess H, Xiao J. A multi-layered protein network stabilizes the *Escherichia coli* FtsZ-ring and modulates constriction dynamics. PLoS Genet 2015;11(4):e1005128.

[56] Del Viso F, Huang F, Myers J, Chalfant M, Zhang Y, Reza N, et al. Congenital heart disease genetics uncovers context-dependent organization and function of nucleoporins at cilia. Dev Cell 2016;38(5):478–92.

[57] Karanastasis AA, Zhang Y, Kenath GS, Lessard MD, Bewersdorf J, Ullal CK. 3D mapping of nanoscale crosslink heterogeneities in microgels. Mater Horiz 2018;5(6):1130–6.

[58] Brown TA, Tkachuk AN, Shtengel G, Kopek BG, Bogenhagen DF, Hess HF, et al. Superresolution fluorescence imaging of mitochondrial nucleoids reveals their spatial range, limits, and membrane interaction. Mol Cell Biol 2011;31(24):4994–5010.

[59] Zhang Y, Schroeder LK, Lessard MD, Kidd P, Chung J, Song Y, et al. Nanoscale subcellular architecture revealed by multicolor three-dimensional salvaged fluorescence imaging. Nat Methods 2020;17(2):225–31.

[60] Kopek BG, Shtengel G, Xu CS, Clayton DA, Hess HF. Correlative 3D superresolution fluorescence and electron microscopy reveal the relationship of mitochondrial nucleoids to membranes. Proc Natl Acad Sci USA 2012;109(16):6136–41.

[61] Sochacki KA, Shtengel G, van Engelenburg SB, Hess HF, Taraska JW. Correlative super-resolution fluorescence and metal-replica transmission electron microscopy. Nat Methods 2014;11(3):305–8.

[62] Li Y, Mund M, Hoess P, Deschamps J, Matti U, Nijmeijer B, et al. Real-time 3D single-molecule localization using experimental point spread functions. Nat Methods 2018;15(5):367–9.

[63] Liu S, Huang F. Enhanced 4Pi single-molecule localization microscopy with coherent pupil based localization. Commun Biol 2020;3(1):220.

[64] Li Y, Buglakova E, Zhang Y, Thevathasan VJ, Bewersdorf J, Ries J. Accurate 4Pi single-molecule localization using an experimental PSF model. Opt Lett 2020;45(13):1–12.

[65] Lakadamyali M, Cosma MP. Visualizing the genome in high resolution challenges our textbook understanding. Nat Methods 2020;17(4):371–9.

[66] Sharonov A, Hochstrasser RM. Wide-field subdiffraction imaging by accumulated binding of diffusing probes. Proc Natl Acad Sci USA 2006;103(50):18911–6.

[67] Jungmann R, Steinhauer C, Scheible M, Kuzyk A, Tinnefeld P, Simmel FC. Single-molecule kinetics and super-resolution microscopy by fluorescence imaging of transient binding on DNA origami. Nano Lett 2010;10(11):4756–61.

[68] Nieves DJ, Gaus K, Baker MAB. DNA-based super-resolution microscopy: DNA-PAINT. Genes 2018;9(12):E621

[69] Chen F, Tillberg PW, Boyden ES. Optical imaging. Expansion microscopy. Science 2015;347(6221):543–8.

[70] Wassie AT, Zhao Y, Boyden ES. Expansion microscopy: principles and uses in biological research. Nat Methods 2019;16(1):33–41.

[71] Balzarotti F, Eilers Y, Gwosch KC, Gynnå AH, Westphal V, Stefani FD, et al. Nanometer resolution imaging and tracking of fluorescent molecules with minimal photon fluxes. Science 2017;355(6325):606–12.

[72] Gwosch KC, Pape JK, Balzarotti F, Hoess P, Ellenberg J, Ries J, et al. MINFLUX nanoscopy delivers 3D multicolor nanometer resolution in cells. Nat Methods 2020;17(2):217–24.

[73] Wang H, Rivenson Y, Jin Y, Wei Z, Gao R, Günaydın H, et al. Deep learning enables cross-modality super-resolution in fluorescence microscopy. Nat Methods 2019;16(1):103–10.

[74] Jin L, Liu B, Zhao F, Hahn S, Dong B, Song R, et al. Deep learning enables structured illumination microscopy with low light levels and enhanced speed. Nat Commun 2020;11(1):1934.

[75] Schlichthaerle T, Strauss MT, Schueder F, Auer A, Nijmeijer B, Kueblbeck M, et al. Direct visualization of single nuclear pore complex proteins using genetically-encoded probes for DNA-PAINT. Angew Chem Int Ed Engl 2019;58(37):13004–8.

[76] Jungmann R, Avendaño MS, Woehrstein JB, Dai M, Shih WM, Yin P. Multiplexed 3D cellular super-resolution imaging with DNA-PAINT and Exchange-PAINT. Nat Methods 2014;11(3):313–8.

[77] Spahn C, Grimm JB, Lavis LD, Lampe M, Heilemann M. Whole-cell, 3D, and multicolor STED imaging with exchangeable fluorophores. Nano Lett 2019;19(1):500–5.

[78] Gao M, Maraspini R, Beutel O, Zehtabian A, Eickholt B, Honigmann A, et al. Expansion stimulated emission depletion microscopy (ExSTED). ACS Nano 2018;12(5):4178–85.

[79] Tong Z, Beuzer P, Ye Q, Axelrod J, Hong Z, Cang H. Ex-STORM: expansion single molecule super-resolution microscopy. bioRxiv049403.

[80] Baddeley D, Batram C, Weiland Y, Cremer C, Birk UJ. Nanostructure analysis using spatially modulated illumination microscopy. Nat Protoc 2007;2(10):2640–6.

[81] Hao X, Allgeyer ES, Lee DR, Antonello J, Watters K, Gerdes JA, et al. Three-dimensional adaptive optical nanoscopy for thick specimen imaging at sub-50-nm resolution. Nat Methods 2021;18(6):688–93.

[82] Curdt F, Herr SJ, Lutz T, Schmidt R, Engelhardt J, Sahl SJ, et al. IsoSTED nanoscopy with intrinsic beam alignment. Opt Express 2015;23(24):30891–903.

[83] Yang X, Xie H, Alonas E, Liu Y, Chen X, Santangelo PJ, et al. Mirror-enhanced super-resolution microscopy. Light Sci Appl 2016;5(6):e16134.

[84] Schnitzbauer J, McGorty R, Huang B. 4Pi fluorescence detection and 3D particle localization with a single objective. Opt Express 2013;21(17):19701–8.

[85] Hao X, Antonello J, Allgeyer ES, Bewersdorf J, Booth MJ. Aberrations in 4Pi microscopy. Opt Express 2017;25(13):14049–58.

[86] Booth MJ. Adaptive optical microscopy: the ongoing quest for a perfect image. Light Sci Appl 2014;3(4):e165.